NANO LETTERS

Letter

pubs.acs.org/NanoLett

Self-Assembled InGaAs Quantum Dot Clusters with Controlled Spatial and Spectral Properties

Megan Creasey,[†] Ji-Hoon Lee,[‡,∥] Zhiming Wang,[§,∥] Gregory J. Salamo,[∥] and Xiaoqin Li*[,†]

[†]Department of Physics, University of Texas at Austin, Austin, Texas 78712, United States

[‡]Department of Electrical Engineering, Kwangwoon University, Seoul, South Korea 139-701

[§]State Key Laboratory of Electronic Thin Films and Integrated Devices, University of Electronic Science and Technology of China, Chengdu, People's Republic of China 610054

[∥]Institute for Nanoscale Science and Engineering, University of Arkansas, Fayetteville, Arkansas 72701, United States

Supporting Information

ABSTRACT: Planar quantum dot clusters (QDCs) consisting of six InGaAs quantum dots (QDs) formed around a GaAs nanomound are the most sophisticated self-assembled QDCs grown by molecular beam epitaxy thus far. We present the first photoluminescence measurements on individual hexa-QDCs with high spatial, spectral, and temporal resolution. In the best QDCs, the excitons confined in individual QDs are remarkably close in energy, exhibiting only a 10 meV spread. In addition, a biexponential decay profile and small variation in decay rates for different QDs was observed. The homogeneous energetics and dynamics suggest that the sizes, shapes, and composition of the QDs within these clusters are highly uniform.

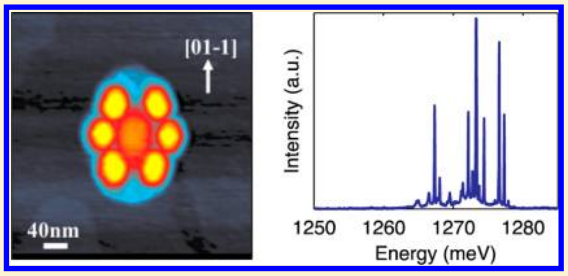

KEYWORDS: *Quantum dot clusters, photoluminescence, exciton lifetime, time-resolved spectroscopy, single dot spectroscopy*

Creating materials from nanobuilding blocks with designed properties represents a fundamental goal of material- and nanoscience. One prominent example of an engineered material is the semiconductor quantum dot (QD), often referred to as an artificial atom. The abundance of studies on QDs over the last two decades has been driven by their unique electrical and optical properties. The carriers inside QDs are confined in all three dimensions and thus have a discrete and tunable energy spectrum as well as relatively long carrier lifetimes. These features make QDs the preferred material for a number of optoelectronic devices, such as lasers and photodetectors with enhanced thermal stability, as well as an enticing platform for building novel quantum information processing devices.[1−3] Further developments in the fabrication of advanced QD structures, like three-dimensional lattices of QDs with controlled spatial and spectral properties, will lead to improved devices such as intermediate-band solar cells.[4]

QDCs, consisting of two or more closely spaced QDs, represent an important step in creating advanced QD configurations.[5] The most frequently studied configuration consists of vertically stacked QDs, which form due to the preferential growth of QDs at the same location as QDs in a buried layer.[6−8] This vertical configuration is attractive because it is relatively easy to grow the QDCs and to vary interactions between QDs by changing the layer spacing. Unfortunately, these QDCs are limited to interactions along one dimension; it is difficult, therefore, to scale beyond two QDs. Alternatively, one may grow QDCs in the same plane, which allows for electrical control and coupling in two-dimensions. Planar QDCs have been grown by a variety of methods such as strain enhanced etching and lithography patterning.[9−13] These methods, however, either involve ex-situ surface preparation or require additional processing steps that add to the complexity of the fabrication processes. Therefore, planar QDCs formed by self-assembly are attractive for their simple growth procedure.

We investigate QDCs produced using molecular beam epitaxy (MBE) by a hybrid growth technique, combining droplet homoepitaxy and Stranski-Krastonov (SK) growth.[14−16] QDCs with several different configurations may be grown using this approach. We focus on hexa-QDCs consisting of six InGaAs QDs formed around a GaAs nanomound, the most sophisticated self-assembled QDCs grown by MBE thus far. Previous experiments on planar QDCs have focused on either growth and structural characterizations or spectroscopy of QD pairs.[10−13,17,18] Spectroscopic studies conducted on individual QDCs with more than two QDs have not been previously reported. Such studies are instrumental in addressing key challenges in controlling the properties of QDCs and evaluating their potential for scalability.

Received: June 8, 2012
Revised: August 31, 2012
Published: September 19, 2012

We present the first photoluminescence measurements on individual hexa-QDCs with high spatial, spectral, and temporal resolution. In some QDCs, we observe six exciton transitions close in energy, exhibiting merely a 10 meV spread, with narrow linewidths (<120 μeV, limited by instrument resolution). The lifetime measurements revealed distinct biexponential decays with approximately a factor of 2 variation between decay constants for different QDs. The similar exciton energetics and dynamics suggest a high degree of uniformity in the size, shape, and composition of the QDs within the cluster. These QDCs with controlled spatial and spectral properties should enable novel applications based on collective electronic excitations and entangled photon emissions.[19] For example, quantum logic devices built with single QDs are limited to one or two-qubit operations. The simplest error-correcting quantum algorithm, however, requires a minimum of 5 qubits.[20,21] QDCs with controlled coupling among constituent QDs clearly offer a solution for building quantum information processing devices with multiple qubits.

We describe the MBE growth briefly. Details of the growth technique have been reported previously.[14,22,23] Epi-ready semi-insulated GaAs (100) was first annealed at 610 °C for 10 min to remove oxides. Following the annealing, a buffer layer of GaAs was grown at a rate of 0.75 monolayers per second (ML/s) at a temperature of 610 °C. The substrate was then annealed a second time for 3 min to reduce surface dislocations. Subsequently, the substrate temperature was lowered to 150 °C, and Ga was introduced into the chamber. This step created liquid Ga droplets via Volmer–Weber growth. The droplets were crystallized into GaAs nanomounds by the introduction of As_4 at a beam equivalent pressure (BEP) of 1.3×10^{-5} Torr. Following the formation of GaAs mounds, the substrate temperature was raised to 500 °C, and 2.0 ML of InAs was deposited under a BEP of 3.4×10^{-6} Torr of As_4, causing SK formation of InAs QDs around the nanomound templates. For optical measurements, an additional 100 nm capping layer of GaAs was grown on top of the QDs.

The number of QDs in each cluster is primarily controlled by the amount of InAs deposited. For this study, 2.0 ML of InAs led to preferential growth of six QDs around each nanomound as shown in Figure 1a. An atomic force microscopy study of a sample grown by the same process, but without a capping layer, found that more than 80% of the QDCs grown by this method contain a nanomound surrounded by six QDs, while close to 7% contain five QDs, and 12% contain four QDs.[14] The measured density of these samples is approximately 5×10^8 QDCs/cm^2.

The hexa-QDCs are slightly elongated along the [01−1] crystal axis. The GaAs nanomound template persists after growth of the QDs as a wide InGaAs mesa with a height of approximately 15 nm. While the whole cluster has a diameter of approximately 150 nm, the individual InGaAs QDs are much smaller, as is evidenced in the lateral profiles in Figure 1b. The precise dimensions of the QDs were difficult to determine as the QDs partially reside on the top of the mound, but we estimate from Figure 1b that the QDs have heights between 9 and 14 nm. Laterally, the QDs are separated by 50 nm from their nearest neighbors.

We performed spectrally and temporally resolved photoluminescence measurements at both ensemble and single cluster levels. The experimental setup is described as the following: The excitation source was a Ti:Sapphire laser tuned to 1520 meV with a pulse duration of ~150 fs and a repetition

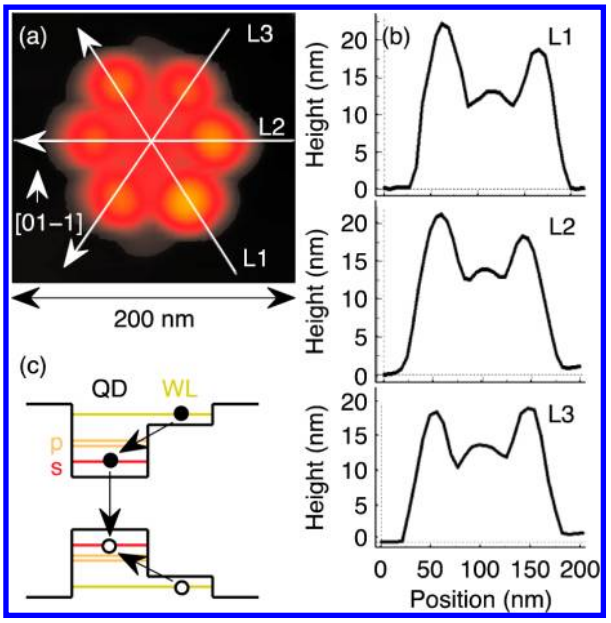

Figure 1. (a) AFM image of uncapped QDC. (b) Cross sections of uncapped QDC along the directions indicated in a. (c) Energy diagram, including bulk GaAs, InGaAs wetting layer, and QDs.

rate of 80 MHz. The beam was focused onto the sample using a microscope objective in a confocal configuration. The excitation spot size was approximately 85 μm in diameter for ensemble measurements and 1.5 μm in diameter for single cluster measurements. After passing through a 0.55 m spectrometer, the photoluminescence was detected with either a Si CCD, for spectrally resolved measurements, or an avalanche photodiode, for temporally resolved measurements. To obtain a good signal-to-noise ratio for the single cluster decay measurements, long integration times (≥1000 s) were necessary. For all of these measurements, the sample was held on the coldfinger of a liquid helium flow cryostat at temperatures between 10 and 20 K.

We first conducted spectrally resolved ensemble measurements at various excitation densities to identify relevant electronic transitions. Several pronounced transitions were observed corresponding to the energy diagram schematically shown in Figure 1c. The wetting layer and bulk GaAs emit at 1470 and 1520 meV, respectively. We did not observe any distinct optical signature specifically related to the GaAs nanomound, which would lead to a spatially localized optical response. We identified the two emission states, shown in Figure 2a, as confined excitons in the QDCs. At the lowest excitation density (≤6.4 W/cm^2) the spectrum has a single peak at 1214 meV with a fwhm of 48 meV. We assign this emission to the exciton ground state, or "s-shell" state.[24] By the highest excitation density used (160 W/cm^2), a very pronounced second peak has emerged. This peak is centered on 1268 meV with a fwhm of 60 meV. Given the nonlinear power dependence and the separation from the first peak of 54 meV, this additional peak is most likely due to the first excited state, or the "p-shell" state. These spectral features are consistent with those observed in extensively investigated SK grown InGaAs QDs.[25−29]

Following spectral characterization, we conducted lifetime measurements for the ensemble on both confined exciton states. The decay dynamics exhibit distinct biexponential behavior. Extracted fast (τ_f) and slow decay (τ_s) components

dx.doi.org/10.1021/nl3021736 | Nano Lett. 2012, 12, 5169−5174

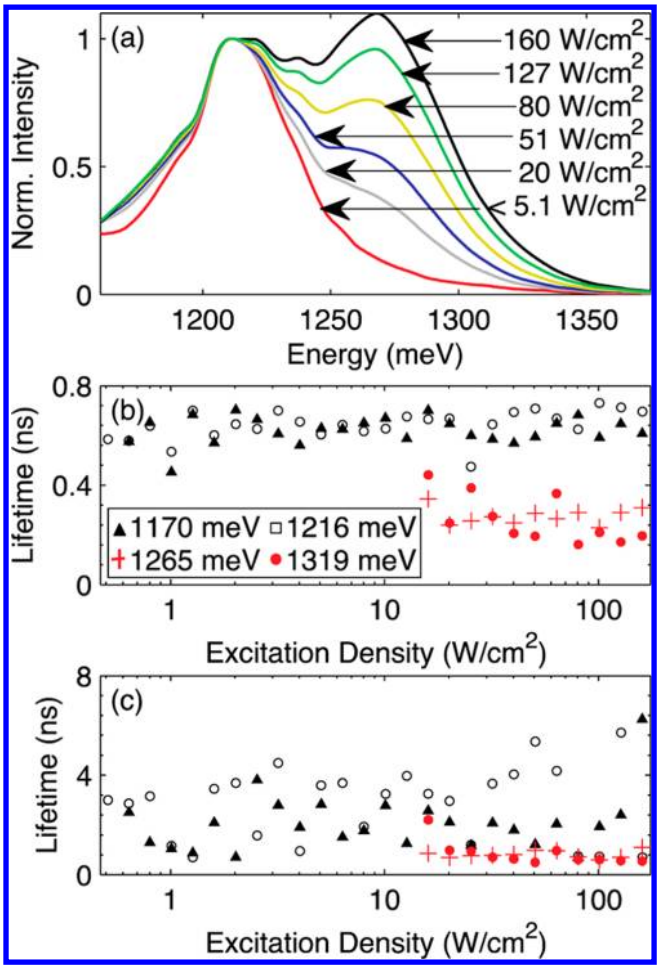

Figure 2. (a) Normalized PL spectra for an ensemble of QDCs. (b) Fast and (c) slow decay times (τ_f and τ_s), for an ensemble of QDCs at different excitation densities. Open black circles and solid black triangles represent lifetime data from the s-shell state with emission energies at 1170 and 1216 meV. Filled red circles and red crosses represent lifetime data from the p-shell state with emission energies at 1265 and 1319 meV.

are shown in Figure 2b and c, respectively. We performed detailed studies of decay constant dependence on emission energy, but for simplicity only two emission energies for each exciton state are displayed in Figure 2b,c. We observed no clear dependence of lifetime on emission energy from either state. While a systematic change of radiative lifetime on emission energy may be expected, the size, shape, composition, and interface quality can easily change the behavior that dominates such trends. Indeed, previous studies have reported contradictory results.[30−39] These discrepancies can be partially accounted for by nonradiative decay, which is often erroneously assumed to be zero or negligible at low temperatures.[31] It is particularly difficult to predict how nonradiative decay should depend on emission energy. Several different nonradiative decay mechanisms, such as interaction with acoustic phonons and surface trap states may be simultaneously present, and each has a different energy dependence. Additionally, we studied how the decay constants depend on the excitation power. The measured fast decay and slow decay were 0.57 ± 0.09 ns and 2.34 ± 1.4 ns, respectively. These statistics were collected at 1170, 1216, 1265, and 1319 meV for pump powers below excitation of the p-shell states. We observed a decrease in the fast decay component (Figure 2b) from 0.6 ns in the s-shell state to 0.2 ns in the p-shell state, which emerges at a higher excitation power. The measured shorter lifetime associated with exciton excited states is consistent with several previous experimental studies on self-assembled InAs QDs and has been explained by additional decay pathways.[40,41]

While ensemble measurements provide statistically averaged information about a large number of clusters, only measurements performed on individual QDCs provide information on the energetics and dynamics of excitons confined in each QD within the cluster. This vital information allows us to evaluate the potential of introducing controlled coupling between QDs. However, the low emission intensity and high density of the QDCs make single cluster measurements very challenging. This study therefore concentrates primarily on spatially isolated clusters at the higher energy end of the ensemble spectrum where Si-based detectors are more efficient. By selecting clusters with higher emission energy, we risk selecting QDCs that are somewhat unique. Ideally, one would characterize the structural and optical properties of the same cluster; however, such correlated measurements are very difficult and frequently require processes that destroy the sample for further use.

For the μPL measurement, the laser was focused onto the sample using a microscope objective to achieve an excitation spot size less than 1.5 μm in diameter. Thus, when we measured a single QDC roughly 1 μm distant from its neighbors, only the QDs inside this cluster were excited. We performed a simple test to ensure that the spectrum was actually from a single cluster. When we moved the excitation spot in small increments (approximately 0.5 μm) away from a QDC of interest, the group of emission lines associated with that QDC simultaneously disappeared as the excitation spot left the QDC. Furthermore, new sets of emission lines with completely different energies did not appear until a new cluster entered the excitation spot. We therefore conclude that such spectra are from a single QDC. Similar approaches have been used in previous studies.[26,42]

Figures 3 and 4 show spectral and temporal information from the same single QDC. A series of spectra taken at different excitation powers is displayed in Figure 3. A single QDC spectrum typically consists of four to six sharp emission lines at low excitation intensity ($\leq$8.6 W/cm^2). The intensities of these transitions have a linear dependence on excitation power and are thus likely due to the exciton ground state (i.e., s-shell state). At higher excitation intensities additional groups of emission lines appear near 1337 meV. These additional lines may be attributed to p-shell transitions in the QDs. Their energy separation from the s-shell states, 60−70 meV, is consistent with that in the ensemble measurements. For many QDCs, an additional third set of emission lines appears at 10−20 meV above the first p-shell transition for excitation powers near 27 W/cm^2. Because of the close proximity of these lines to the original p-shell states, these states present themselves as a broadening of the transition in the ensemble measurements, not as a third peak. We tentatively assign these emission lines as additional p-shell transitions. A "p-p" splitting of tens of meV may arise from alloy fluctuations and shape anisotropy.[40,43] Emissions at lower energy than the exciton ground states (not pictured) are also observed at higher excitation powers. These states have been observed in previous studies performed on single InAs QDs grown by the SK method.[25,27] It has been suggested that these states arise from interaction between the band-filled wetting layer and the state-filled QD.[44] A precise

dx.doi.org/10.1021/nl3021736 | Nano Lett. 2012, 12, 5169−5174

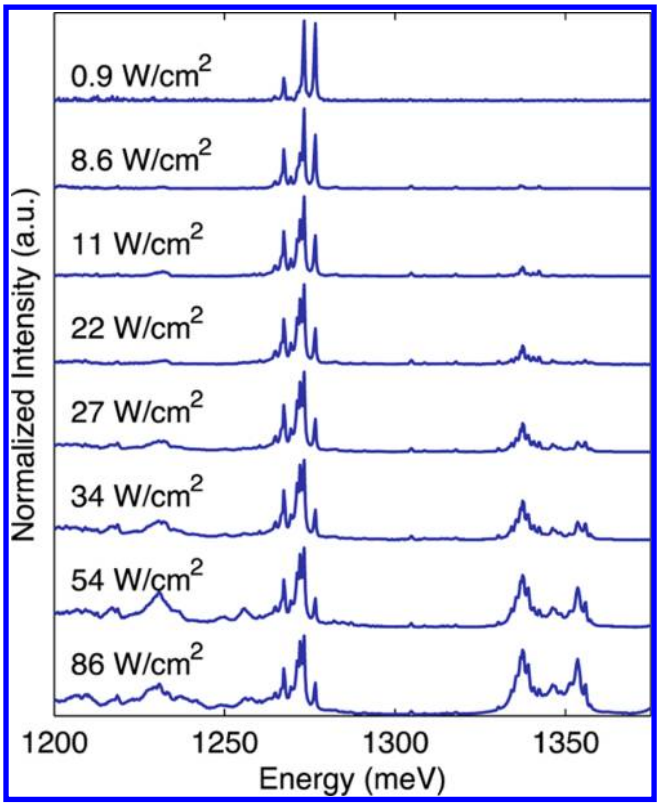

Figure 3. Normalized excitation density-dependent μPL for a single QDC.

analysis of the power dependence of PL intensity from the states other than s-shell states was complicated by the emergence of new peaks and the spectral broadening.

Figure 4a displays a high resolution spectrum of the same cluster at low excitation power (8.6 W/cm^2) showing six closely spaced emission lines at 1267.4 meV (A), 1272.2 meV (B), 1273.3 meV (C), 1274.4 meV (D), 1276.6 meV (E), and 1277.3 meV (F). The other weak peaks present in the spectrum are spatially localized and associated with the same QDC. We suggest that they may arise from trions or biexcitons. The very small variation in emission energy suggests that the QDs in this particular QDC have a very uniform size, shape, and composition. These transitions (A–F) all exhibit narrow linewidths ≤0.1 meV, corresponding to a long dephasing time, similar to that measured in InAs QD molecules previously.[45] The narrow energy distribution and long dephasing time of QDs within a single cluster make these QDCs particularly attractive for quantum information applications. In previous studies on QD pairs with an average interdot distance of tens of nanometers, applied in-plane electric fields were used to couple exciton transitions separated by a few meV.[10−12] Such controlled coupling between QDs is critical for scalable quantum logic operations or entangled photon generation. In addition, the narrow energy distribution could also be exploited to create a single photon source continuously tunable over a relatively large wavelength range via a small temperature variation when the hexa-QDCs are placed in photonic nanowires.[46]

We further investigate exciton dynamics of each of the six transitions. An example of the decay dynamics from C, the strongest emission line, is displayed in Figure 4b. The time correlated single photon counting (TCSPC) measurements

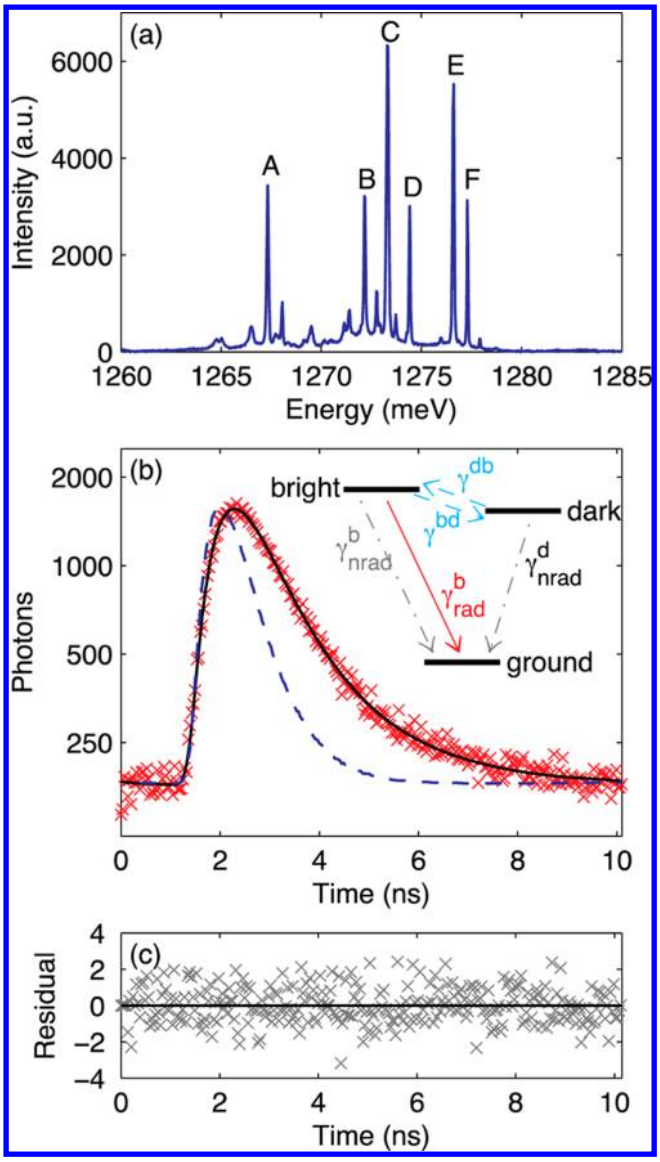

Figure 4. (a) High resolution μPL of the QDC shown in Figure 3. Labels correspond to emission energies referenced in the text. (b) TCSPC histogram for emission line C. Raw data is shown as red Xs. Dashed blue line shows the instrument response function (IRF). Black line shows a biexponential fit convolved with the IRF. Inset: schematic of a three-level system involving the crystal ground state, the bright exciton state, and a dark state. (c) Normalized residual for the biexponential fit to b.

were made using an excitation intensity of 8.6 W/cm^2, below saturation of the s-shell, to prevent any possible biexciton contribution from complicating the measurement. The decay histograms were fit with three models, a single exponential, a single exponential with a delayed rise time, and a biexponential decay. The biexponential model provided the best fit to the data with a reduced χ^2 value of 1.01, whereas the other models were poorer fits with values of 3.08 and 2.98, respectively. The failure of the delayed rise time model indicates very fast rise times, below the 60 ps resolution of the measurement. This suggests that photoexcited carriers are quickly thermalized to the lowest available exciton state. At the low excitation power used in this measurement, we did not observe any signature of the exciton dynamics arising from the cascaded biexciton decay. Typically, such cascaded processes lead to a delayed rise time

dx.doi.org/10.1021/nl3021736 | Nano Lett. 2012, 12, 5169−5174

due to the finite relaxation time of carriers leaving other states.[40,47−49] The fast rise times also suggest that there is no carrier transfer between QDs in the clusters on time scales detectable with our experimental setup.

The excellent agreement between the data and the biexponential fit is evident from the random distribution of the normalized residual shown in Figure 4c. The chosen biexponential fit is written explicitly as:

$$I(t) = P_0 + \frac{P_f}{\tau_f} e^{-(t-t_0)/\tau_f}\Theta(t - t_0) + \frac{P_s}{\tau_s} e^{-(t-t_0)/\tau_s}\Theta(t - t_0) \quad (1)$$

where P_0 is the background intensity, t_0 is the initial rise time, $P_{f/s}$ is the intensity of the fast (slow) decay, $\tau_{f/s}$ is the decay time of the fast (slow) signal, and $\Theta(t)$ is the Heaviside step function. Equation 1 was convolved with a histogram taken of the laser on a reflective surface to correct for the instrument response function of the electronics. The convolved fit was matched to the raw data using a Levenberg−Marquardt algorithm. For this specific resonance, a fast decay of 0.44 ns and a slow decay of 1.70 ns were extracted. All other resonances within this QDC exhibit similar biexponential decays. The measured decay lifetimes are summarized in Table 1. The similar decay parameters of all resonances suggest that there is no significant carrier tunneling and incoherent energy relaxation among QDs. Both of these coupling mechanisms would lead to a faster decay time for higher energy states.[12]

Table 1. Exciton Decay Constants for Each QD in a Single QDC with Excellent Homogeneity

emission line	energy (meV)	τ_f (ns)	τ_s (ns)
A	1267.4	0.284	1.51
B	1272.2	0.206	1.70
C	1273.3	0.442	1.70
D	1274.4	0.298	1.11
E	1276.6	0.400	2.30
F	1277.3	0.382	2.41

A simple two-level model cannot explain the biexponential dynamics. A three-level model, as shown in Figure 4b, including a nonradiative exciton dark state or trap state is needed to explain this experimental observation. We assume that the radiative (γ_{rad}^{b}) and nonradiative (γ_{nrad}^{b}) decay rates of the bright state and the nonradiative (γ_{nrad}^{d}) decay rate of the dark state are much faster than the bright-dark state transfer rates (γ^{bd} and γ^{db}). As a result, the fast decay rate is determined by $\gamma_f = 1/\tau_f = \gamma_{rad}^{b} + \gamma_{nrad}^{b}$, and the slow decay rate is determined by $\gamma_s = 1/\tau_s = \gamma_{nrad}^{d}$. We emphasize that this interpretation of the fast and slow decay component is a simplification under the assumption of long dark-bright state transfer rates. The decay of the dark state can only be monitored following the dark-bright state transfer. Biexponential dynamics on similar time scales involving dark excitons have been observed in ensembles of SK InAs QDs.[50] The exact nature of the dark state in our QDCs is unclear without further spectroscopic study, but given that the slow decay component exhibits large variations across the sample in ensemble measurements, we suggest that the dark state may be related to trap or defect states.

In summary, we conducted the first photoluminescence measurements on single InGaAs hexa-QDCs with high spatial, spectral, and temporal resolutions. The spectra collected from individual QDCs show four to six strong, narrow transitions per cluster. In some cases, the resonant energies for excitons confined in the same cluster are remarkably close, exhibiting approximately a 10 meV spread. Exciton lifetime measurements reveal a distinct biexponential behavior. The fast decay component is typically below 0.5 ns, and the slow component is above 1 ns. The dynamic parameters describing the exciton transitions vary by approximately a factor of 2. These lifetimes are comparable with those observed in the extensively investigated SK-grown InAs QDs. We describe the biexponential decay dynamics with a three-level model consisting of a ground state, a bright exciton state, and a dark state. Under certain assumptions, we can assign the fast decay rate as the total decay rate of the bright state and the slow decay rate as the nonradiative decay rate of the dark state. The uniform exciton energetics and dynamics make these QDCs ideal for potential applications such as tunable photon sources and quantum logic gates. However, QDs within a cluster are likely uncoupled, as grown, due to the large spatial separation between them. We propose applying an in-plane electric field to induce coupling in a controllable manner. In addition, it would be interesting to investigate possible dynamic changes as the number of QDs in a single cluster varies. To achieve this goal, one may study a series of samples with varied numbers of QDs in a single QDC by changing the indium flux during the growth process. These experiments have the potential to facilitate a sophisticated understanding of exciton dynamics in QDs while developing novel technologies for future engineered quantum systems.

■ ASSOCIATED CONTENT

Supporting Information

Raw images showing that optical spectra are taken from individual QDCs. Additional QDC spectra, single QD lifetime data, and related statistics. This material is available free of charge via the Internet at http://pubs.acs.org.

■ AUTHOR INFORMATION

Corresponding Author

*E-mail: elaineli@physics.utexas.edu.

Notes

The authors declare no competing financial interest.

■ ACKNOWLEDGMENTS

We gratefully acknowledge financial support from the following sources: NSF DMR-0747822, ONR N00014-08-1-0745, Welch Foundation F-1662, AFOSR FA9550-10-1-0022, ARO-W911NF-08-1-0348, and the Alfred P. Sloan Foundation. Prof. Jihoon Lee is supported in part by the Basic Science Program through the National Research Foundation (NRF) of Korea funded by the Ministry of Education, Science and Technology (Grant Nos. 2010-0008394 and 2011-0030821).

■ REFERENCES

(1) Li, X. Q.; Wu, Y. W.; Steel, D.; Gammon, D.; Stievater, T. H.; Katzer, D. S.; Park, D.; Piermarocchi, C.; Sham, L. J. *Science* **2003**, *301*, 809−811.

(2) Kim, D.; Carter, S. G.; Greilich, A.; Bracker, A. S.; Gammon, D. *Nat. Phys.* **2011**, *7*, 223.

(3) Robledo, L.; Elzerman, J. M.; Jundt, G.; Atatüre, M.; Högele, A.; Fält, S.; Imamoğlu, A. *Science* **2008**, *320*, 772.

(4) Martí, A.; Antolín, E.; Stanley, C. R.; Farmer, C. D.; López, N.; Díaz, P.; Cánovas, E.; Linares, P. G.; Luque, A. *Phys. Rev. Lett.* **2006**, *97*, 247701.

(5) Kiravittaya, S.; Rastelli, A.; Schmidt, O. G. *Rep. Prog. Phys.* **2009**, *72*, 046502.
(6) Krenner, H. J.; Sabathil, M.; Clark, E. C.; Kress, A.; Schuh, D.; Bichler, M.; Abstreiter, G.; Finley, J. J. *Phys. Rev. Lett.* **2005**, *94*, 057402.
(7) Bayer, M.; Hawrylak, P.; Hinzer, K.; Fafard, S.; Korkusinski, M.; Wasilewski, Z. R.; Stern, O.; Forchel, A. *Science* **2001**, *291*, 451−453.
(8) Colocci, M.; Vinattieri, A.; Lippi, L.; Bogani, F.; Rosa-Clot, M.; Taddei, S.; Bosacchi, A.; Franchi, S.; Frigeri, P. *Appl. Phys. Lett.* **1999**, *74*, 564−566.
(9) Songmuang, R.; Kiravittaya, S.; Schmidt, O. G. *Appl. Phys. Lett.* **2003**, *82*, 2892.
(10) Beirne, G. J.; Hermannstädter, C.; Wang, L.; Rastelli, A.; Schmidt, O. G.; Michler, P. *Phys. Rev. Lett.* **2006**, *96*, 137401.
(11) Wang, L.; Rastelli, A.; Kiravittaya, S.; Atkinson, P.; Ding, F.; Bof Bufon, C. C.; Hermannstädter, C.; Witzany, M.; Beirne, G. J.; Michler, P.; Schmidt, O. G. *New J. Phys.* **2008**, *10*, 045010.
(12) Hermannstädter, C.; Beirne, G. J.; Witzany, M.; Heldmaier, M.; Peng, J.; Bester, G.; Wang, L.; Rastelli, A.; Schmidt, O. G.; Michler, P. *Phys. Rev. B* **2010**, *82*, 085309.
(13) Peng, J.; Hermannstädter, C.; Witzany, M.; Heldmaier, M.; Wang, L.; Kiravittaya, S.; Rastelli, A.; Schmidt, O. G.; Michler, P.; Bester, G. *Phys. Rev. B* **2010**, *81*, 205315.
(14) Lee, J. H.; Sablon, K.; Wang, Z. M.; Salamo, G. J. *J. Appl. Phys.* **2008**, *103*, 054301.
(15) Yakes, M. K.; Cress, C. D.; Tischler, J. G.; Bracker, A. S. *ACS Nano* **2010**, *4*, 3877−3882.
(16) Creasey, M.; Li, X.-Q.; Lee, J. H.; Wang, Z. M.; Salamo, G. J. *J. Appl. Phys.* **2010**, *107*, 104302.
(17) Unold, T.; Mueller, K.; Lienau, C.; Elsaesser, T.; Wieck, A. D. *Phys. Rev. Lett.* **2005**, *94*, 137404.
(18) Liang, B. L.; Wang, Z. M.; Wang, X. Y.; Lee, J. H.; Mazur, Y. I.; Shih, C. K.; Salamo, G. J. *ACS Nano* **2008**, *2*, 2219−2224.
(19) Economou, S.; Linder, N.; Rudolph, T. *Phys. Rev. Lett.* **2010**, *105*, 093601.
(20) Bennett, C.; DiVincenzo, D.; Smolin, J.; Wootters, W. *Phys. Rev. A* **1996**, *54*, 3824−3851.
(21) Laflamme, R.; Miquel, C.; Paz, J. P.; Zurek, W. H. *Phys. Rev. Lett.* **1996**, *77*, 198−201.
(22) Lee, J. H.; Wang, Z. M.; Strom, N. W.; Mazur, Y. I.; Salamo, G. J. *Appl. Phys. Lett.* **2006**, *89*, 202101.
(23) Sablon, K.; Lee, J. H.; Wang, Z. M.; Shultz, J. H.; Salamo, G. J. *Appl. Phys. Lett.* **2008**, *92*, 203106.
(24) The lower energy shoulder only appeared after the data was corrected for the wavelength dependent quantum efficiency of the CCD. It is likely an artifact due to inaccurate quantum efficiency calibration in this wavelength range.
(25) Bayer, M.; Stern, O.; Hawrylak, P.; Farad, S.; Forchel, A. *Nature* **2000**, *405*, 923−926.
(26) Dekel, E.; Gershoni, D.; Ehrenfreund, E.; Spektor, D.; Garcia, J. M.; Petroff, P. M. *Phys. Rev. Lett.* **1998**, *80*, 4991−4994.
(27) Dekel, E.; Gershoni, D.; Ehrenfreund, E.; Garcia, J. M.; Petroff, P. M. *Phys. Rev. B* **2000**, *61*, 11009.
(28) Grundmann, M.; Bimberg, D. *Phys. Rev. B* **1997**, *55*, 9740−9745.
(29) Malik, S.; Le Ru, E. C.; Childs, D.; Murray, R. *Phys. Rev. B* **2001**, *63*, 155313.
(30) Johansen, J.; Stobbe, S.; Nikolaev, I. S.; Lund-Hansen, T.; Kristensen, P. T.; Hvam, J. M.; Vos, W. L.; Lodahl, P. *Phys. Rev. B* **2008**, *77*, 073303.
(31) Stobbe, S.; Johansen, J.; Kristensen, P. T.; Hvam, J. M.; Lodahl, P. *Phys. Rev. B* **2009**, *80*, 155307.
(32) Wimmer, M.; Nair, S. V.; Shumway, J. *Phys. Rev. B* **2006**, *73*, 165305.
(33) Campbell-Ricketts, T. E. J.; Kleemans, N. A. J. M.; Nötzel, R.; Silov, A. Y.; Koenraad, P. M. *Appl. Phys. Lett.* **2010**, *96*, 033102.
(34) Albert, F.; Stobbe, S.; Schneider, S.; Heindel, T.; Reitzenstein, S.; Höfling, S.; Lodahl, P.; Worschech, L.; Forchel, A. *Appl. Phys. Lett.* **2010**, *96*, 151102.
(35) Stobbe, S.; Schlereth, T. W.; Höfling, S.; Forchel, A.; Hvam, J. M.; Lodahl, P. *Phys. Rev. B* **2010**, *82*, 233302.
(36) Zhang, Y. C.; Pancholi, A.; Stoleru, V. G. *Appl. Phys. Lett.* **2007**, *90*, 183104.
(37) Mazur, Y. I.; Tomm, J. W.; Petrov, V.; Tarasov, G. G.; Kissel, H.; Wather, C.; Zhuchenko, Z. Y.; Masselink, W. T. *Appl. Phys. Lett.* **2001**, *78*, 3214.
(38) Tackeuchi, A.; Nakata, Y.; Muto, S.; Sugiyama, Y.; Usuki, T.; Nishikawa, Y.; Yokoyama, N.; Wada, O. *Jpn. J. Appl. Phys.* **1995**, *34*, 1439.
(39) Wang, C. F.; Badolato, A.; Wilson-Rae, I.; Petroff, P. M.; Hu, E. L.; Urayama, J.; Imamo\v glu, A. *Appl. Phys. Lett.* **2004**, *85*, 3423−3425.
(40) Dekel, E.; Regelman, D. V.; Gershoni, D.; Ehrenfreund, E.; Schoenfeld, W. V.; Petroff, P. M. *Phys. Rev. B* **2000**, *62*, 11038−11045.
(41) Yu, H.; Lycett, S.; Roberts, C.; Murray, R. *Appl. Phys. Lett.* **1996**, *69*, 4087.
(42) Petroff, P. M.; Lorke, A.; Imamoğlu, A. *Phys. Today* **2001**, *54*, 46.
(43) Narvaez, G. A.; Bester, G.; Zunger, A. *J. Appl. Phys.* **2005**, *98*, 043708.
(44) Landin, L.; Miller, M. S.; Pistol, M. E.; Pryor, C. E.; Samuelson, L. *Science* **1998**, *280*, 262−264.
(45) Borri, P.; Langbein, W.; Woggon, U.; Schwab, M.; Bayer, M.; Fafard, S.; Wasilewski, Z.; Hawrylak, P. *Phys. Rev. Lett.* **2003**, *91*, 267401.
(46) Bleuse, J.; Claudon, J.; Creasey, M.; Malik, N. S.; Gérard, J. M.; Maksymov, I.; Hugonin, J. P.; Lalanne, P. *Phys. Rev. Lett.* **2011**, *106*, 103601.
(47) Bacher, G.; Weigand, R.; Seufert, J.; Kulakovskii, V. D.; Gippius, N. A.; Forchel, A.; Leonardi, K.; Hommel, D. *Phys. Rev. Lett.* **1999**, *83*, 4417−4420.
(48) Santori, C.; Solomon, G. S.; Pelton, M.; Yamamoto, Y. *Phys. Rev. B* **2002**, *65*, 073310.
(49) Patton, B.; Langbein, W.; Woggon, U. *Phys. Rev. B* **2003**, *68*, 125316.
(50) Johansen, J.; Julsgaard, B.; Stobbe, S.; Hvam, J. M.; Lodahl, P. *Phys. Rev. B* **2010**, *81*, 081304.